

Semi-Empirical Metrics to Measure the Effects of Large Satellite Constellations on Astronomy

Doyle Hall
Omitron, Inc., Colorado Springs, CO

1 SUMMARY

Several commercial organizations have recently launched or plan to launch constellations containing hundreds or even thousands of Earth-orbiting satellites. Such large constellations can adversely affect astronomical observations [1-3]. This study formulates a set of metrics that assess in different ways the potential impact of light pollution from different constellations on ground-based astronomy. These include the time-averaged expected number of visible and illuminated satellites above a ground-based observer, the fluxes emitted by these satellites, and a brief description of the associated probabilities of astronomical target contamination. The analysis also estimates the statistically expected number of satellites above a ground-based observer that are also expected to be brighter than the currently recommended limit for constellations — a metric that summarizes the potential effect of a large constellation on visible and near-IR spectral band ground-based observations, by simultaneously incorporating the combined effects of population, altitude, brightness, and variability. This composite metric provides a means to evaluate a proposed constellation's potential to affect ground-based astronomy too severely, using a quantitative two-part test that incorporates both relative and absolute evaluation criteria. For existing constellations, the evaluation can be based on actual photometric brightness measurements, which are available in a web-accessible database for many constellation satellites [4-6]. For proposed or planned constellations, a semi-empirical approach can be used, which estimates satellite brightnesses before launch by adjusting those observed for a set of currently orbiting analog satellites, scaling appropriately for differences in satellite sizes, altitude, etc.

2 INTRODUCTION

The primary missions of the NASA Conjunction Assessment Risk Analysis (CARA) team include assessing and mitigating collision risks for a specific set of high value Earth-orbiting satellites [7], as well as establishing and documenting associated methods [8]. However, the “NASA Spacecraft Conjunction Assessment and Collision Avoidance Best Practices Handbook” also provides guidance on other related matters, including the following specific recommendation for owners and operators of satellite constellations [8]:

“If the constellation, given its population, orbit, and constituent satellites, is likely to affect ground-based astronomy, reassign the satellite orbits or modify the satellite construction to eliminate this effect.”

This study aims to develop a single composite metric, or small set of metrics, designed specifically to help make this assessment. The analysis focuses on the visible and near-IR spectral bands, for which the brightness of typical satellites is dominated by reflected sunlight. The methodology is semi-empirical, incorporating brightnesses of constellation satellites recently measured by ground-based sensors, combined with a semi-analytical model of the associated effects on astronomical observers.

Evaluations to assess potential light pollution risk must often be made in the definition phase of a constellation's development, in the absence of a specific or durable spacecraft design, or while the total number of satellites is still being established in design trade studies. In such pre-launch situations, using high fidelity modeling and simulation methods to estimate the brightnesses of the deployed constellation is not feasible, because the parameters required for the analysis are not available. Instead, a semi-empirical approach based on currently orbiting analog satellites can be used for light pollution risk evaluations and design trade studies.

2.1 Overview of Astronomical Light Pollution from Large Constellations

Several commercial organizations have recently launched or plan to launch constellations containing hundreds or even thousands of Earth-orbiting satellites. Such large constellations can adversely affect astronomical observations, such as wide-field imaging in the visible and near-IR spectral bands [1-3]. Several variables contribute to a constellation's overall potential impact on ground-based optical astronomy. These can be divided into two broad classes: constellation parameters and observational system parameters. Constellation parameters include the total number of satellites, the magnitude and variability of the brightness of the individual satellites, as well as the constellation's altitude and other orbital parameters. Observation system parameters include the modality (e.g.,

wide-field imaging, narrow-field imaging, spectroscopy, etc.), the observatory location, the time criticality of the measurements, the required exposure times, as well as the capability of the sensors to schedule and perform mitigations such as mid-exposure interruptions. A wide array of metrics have been developed to measure the impact of constellations on ground-based astronomy [1], including (but not limited to) the number of visible or illuminated constellation satellites above an observatory, their effective stellar magnitudes, their capacity and frequency of glinting in reflected sunlight, and their angular drift rates across sensor apertures and detector arrays. These quantities also can change significantly throughout twilight and nighttime periods, which increases the number of potential diagnostic metrics even further. This wide array of metrics reflects the multivariate nature of the large constellation light pollution analysis problem. Unfortunately, in the regulatory decision process to approve or evaluate proposed constellations, such an overwhelmingly wide array of information can hinder or even prevent the decision making process. This study focuses on developing a single semi-empirical metric (or small set of metrics) designed to provide decision makers a summarized method of comparing the overall impact of different constellations, both current and proposed.

The astronomical community has already analyzed the potential effects of satellite constellations in some detail, and developed a wide array of quantitative metrics to measure their impact [1, 2]. Of course, the brightness of individual constellation satellites represents one of the most important of these metrics. One of the specific recommendations of a the recent *SatCon-1 Workshop Report* “Impact of 3Constellations on Optical Astronomy and Recommendations Toward Mitigations” is that sunlight reflected from individual constellation satellites should be no brighter than a threshold visual magnitude given by [2]

$$M_t = 7.0 + 2.5 \log_{10}(h/(550 \text{ km})) \quad (1)$$

with h indicating the orbital altitude. Section 4 below presents actual ground-based brightness measurements for three currently orbiting constellations, and compares both the median and the level of variability to this established threshold. (In this discussion, magnitudes that are brighter than the limit given by eq. (1) are referred to as “brighter-than-recommended”, for brevity.)

Other metrics previously developed to assess the impact of constellations include the number of visible or illuminated constellation satellites above an observatory, and their angular drift rates across sensor apertures and detector arrays [1, 2]. Section 5 of this analysis also formulates expressions to estimate the number of visible and illuminated satellites above an observer, using both realistic non-uniform distributions of constellation satellites, as well as less realistic uniform distributions. The formulation is then extended to estimate the associated total flux of photons from the constellation incident on a ground-based observer. Finally, the analysis estimates the statistically expected number of satellites above a ground-based observer that are also expected to be brighter than the currently recommended limit given by eq. (1) — a composite metric that incorporates the effects of constellation population, altitude, brightness, variability, and other parameters.

2.2 Two Key Constellation Light Pollution Evaluation Parameters

In particular, two key parameters must be considered when evaluating the potential impact of constellations on visible and near-IR ground-based astronomy: the orbital altitude of the satellites, h , and the solar depression angle, α (also denoted as SDA), which measures how far the Sun is below a ground-based observer’s local horizon [2, 3]. Sunset and sunrise occur when $\alpha = 0$. Three periods of twilight are defined as follows:

- Civil twilight: $0^\circ \leq \alpha < 6^\circ$
- Nautical twilight: $6^\circ \leq \alpha < 12^\circ$
- Astronomical twilight: $12^\circ \leq \alpha < 18^\circ$

Astronomical night spans periods when $\alpha \geq 18^\circ$, which is often the most valuable and productive time to conduct ground-based observations, especially for faint targets, because of the low level of sky foreground contamination. Unfortunately, high-altitude constellations can remain illuminated by sunlight well into astronomical night, and therefore represent a significant potential threat to visible and near-IR ground-based astronomy [1-3]. The composite risk-assessment metrics and the constellation light pollution evaluation tests developed in this analysis explicitly incorporate both h and α as key parameters.

3 CONSTELLATION PARAMETERS

Current and proposed constellations typically contain a large number of identical (or nearly identical) satellites, occupying low-eccentricity orbits at nearly the same altitude and inclination, but distributed in multiple orbital planes. Table 1 shows representative parameters for three partially- or fully-deployed constellations, studied as

example cases in this analysis. Among these, the most populous is the first phase of the SpaceX company’s Starlink constellation, which plans to include 1,440 satellites at an altitude of 550 km, although later phases may include more satellites at other altitudes [9]. The OneWeb constellation plans to include 648 satellites at a higher altitude of 1,200 km [1]. The less populous Iridium 2nd Generation constellation currently has 66 operational satellites with nine on-orbit spares, for a total of 75 orbiting at an altitude of 780 km [10].

Table 1 also lists the recommended brightness threshold magnitudes [2], calculated using eq. (1), which can be compared to actual ground-based brightness measurements for these three constellations.

Table 1. Parameters for the Three Studied Constellations

Constellation Name	Number of Satellites N_c	Orbital Altitude (km) h	Inclination (°) i	Threshold Magnitude M_t
Starlink	1,440	550	53.0	7.00
OneWeb	648	1200	87.9	7.85
Iridium 2 nd Gen.	75	780	86.4	7.38

4 OBSERVED CONSTELLATION SATELLITE BRIGHTNESSES

Extensive photometric observations of many currently orbiting constellation satellites have been conducted recently [2-6]. These include those acquired by the Mini-MegaTORTORA (MMT) automated observatory in Russia, which measures clear-filter photometric magnitudes that are roughly equivalent to V-band measurements [4]. Observational analyses using MMT data have been conducted for both the OneWeb constellation [5], and for the Starlink constellation [6], with the latter focusing on the most recent “VisorSat” design for Starlink satellites, incorporating specific manufacturing modifications to reduce the amount of sunlight reflected towards ground-based observers [7]. MMT temporal light-curve data for these constellations, and an extensive array of other satellites, can be obtained from the <http://mmt9.ru/satellites/> website [4-6].

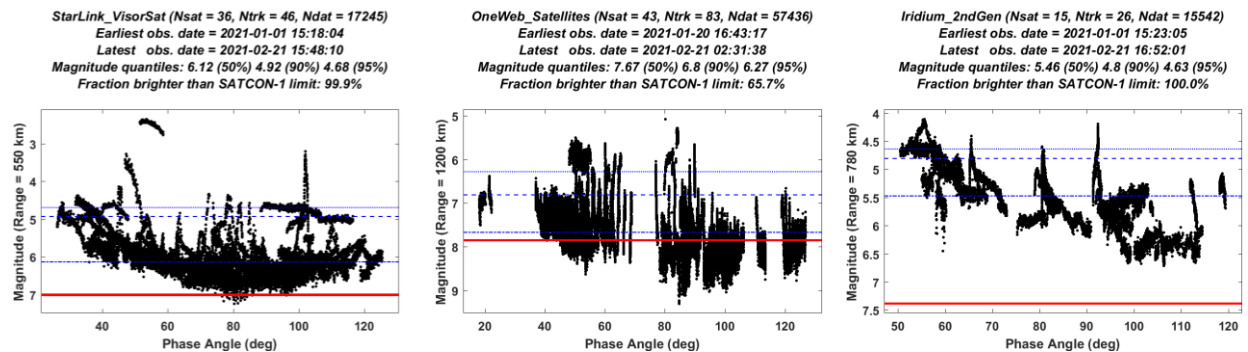


Figure 1. Zenith range-normalized magnitudes measured by the MMT facility [4-6] for satellites from the Starlink (left), OneWeb (middle), and Iridium 2nd Generation (right) constellations. The horizontal red lines show the corresponding recommended maximum brightness magnitudes [2] from eq. (1). The horizontal blue lines show the 50%, 90% and 95% quantiles of the distributions.

Figure 1 shows multiple MMT light-curves for each of the three studied constellations, plotted as a function of solar phase angle (i.e., the observer-satellite-sun angle). Each data set includes observations of 15 or more distinct constellation satellites, and a much larger number of individual photometric measurements (each represented by a black dot). Each individual light-curve (i.e., track) is measured during a single traversal of a satellite over the observatory, and appears in Figure 1 as a coherent, nearly continuous groups of black dots (one such light-curve can be identified relatively easily near the top of the leftmost panel). These data sets are not intended to represent a comprehensive profile of ground-based photometric brightnesses of the constellation satellites. Instead, they represent a subset the available MMT data, observed during the first two months of 2021. Light-curves for Starlink were restricted to VisorSat design satellites [6-8]. In addition, data selected for all three constellations only includes light-curves measured after the satellites had finished maneuvering up to their final, operational orbital altitudes. No other selection criterial were imposed, in an attempt to obtain a representative initial statistical characterization of the overall brightness and variability of satellites in each constellation’s operational configuration. In summary, the plots in Figure 1, represent brightnesses measured for the nearly identical satellites within each constellation, while orbiting at their operational altitudes.

4.1 Zenith Range-Normalized Satellite Magnitudes

Each plot in Figure 1 shows photometric brightnesses in stellar magnitudes, normalized to a satellite range equal to that of the orbital altitude of the constellation, h , as well as to a solar range of one astronomical unit (AU = 1.496×10^8 km). Specifically, the normalized magnitude for a single photometric observation can be calculated from the calibrated exo-atmospheric MMT magnitude, m , using the following adjustment

$$M_z = m - 5 \log_{10}(\rho_o/h) - 5 \log_{10}(\rho_s/AU) \quad (2)$$

with ρ_o indicating the observer-to-satellite range at the time of the observation, and ρ_s the corresponding Sun-to-satellite range. The adjustment for solar range is typically much smaller than that for observer range.

For a satellite directly above a ground-based observer, along the zenith direction, the observer-to-satellite range equals the orbital altitude (neglecting the relatively minor effects of the observatory's elevation and Earth's oblateness). For this reason, this analysis refers to M_z defined in eq. (2) as the "zenith range-normalized magnitude" or just the "zenith magnitude" for brevity, which has been used in previous analyses as a metric for the brightness of individual constellation satellites [1, 5, 6].

4.2 Satellite Brightness Variations

For all but the simplest of objects (e.g., calibration spheres), the brightness of a manufactured satellite in reflected sunlight represents a complex function of a large number of parameters. These can be broadly divided into three categories: observational, environmental and satellite parameters. Observational parameters include time-dependent geometrical variations, such as observer-to-satellite range, solar phase angle, etc. Usually, environmental parameters, such as the illuminating solar flux or atmospheric absorption, are either well known or can be accounted for accurately as part of the photometric calibration process. Satellite parameters can be further subdivided into two categories: attitude and body parameters [9]. Attitude parameters specify the time-dependent inertial orientation of the satellite itself and its articulating components, and provide the means to convert between the inertial reference frame and the body-fixed reference frame. Body parameters comprise all of the information required to calculate the radiant intensity of the object from within the body-fixed reference frame, including parameters describing the shape of the satellite, as well as the reflectance characteristics of the materials covering the outer surfaces. As Figure 1 indicates, this large number of satellite-specific parameters along with variations in observation and illumination geometry together create significant variability in ground-based brightness measurements for actual satellites. Modeling or analyzing the nature and causes of these variations can be labor intensive, and is beyond the scope of this study. Instead, this analysis uses an approach that relies on statistically characterizing the brightnesses of current (and future) constellation satellites.

4.3 Statistical Characterization of Constellation Satellite Magnitudes

The representative data sets plotted in Figure 1 empirically demonstrate that photometric brightnesses vary significantly for all three of the observed constellations, and are likely to vary similarly for future constellations. Specifically, zenith magnitudes are observed to vary with time in two ways: both within individual light-curves — often caused by occasional specular glints of sunlight from satellite components — as well as over longer time scales, i.e., from light-curve to light-curve — which can be caused by satellite attitude or shape configuration changes. For instance, Starlink satellites employ at least two different attitude/shape configurations, called the "open-book" and "shark-fin" modes, known to create significantly different brightnesses recorded by ground-based sensors [2, 11].

Figure 1 indicates the existence of brightness variation trends as a function of solar phase-angle, which are significant but do not dominate the overall variability, except for perhaps in the Iridium 2nd Gen. constellation. No effort is made in this analysis to account for variations with phase angle, although this (and other observational geometric considerations) could be incorporated into future studies using a similar methodology.

This analysis statistically characterizes constellation satellite brightnesses using three quantiles of the observed distributions: the 50% quantile (i.e., the median magnitude), for which 50% of the measurements have dimmer magnitudes, as well as the 90% and 95% quantiles, which serve as dual indicators of both the prevalence and amplitude of upward brightness variations. Figure 1 shows these three quantile magnitudes (denoted here as M_z^{50} , M_z^{90} and M_z^{95} , respectively) plotted as horizontal blue lines over the photometric data. In general, for constellations that have few upward excursions in brightness, whether due to less frequent glinting or the use of less reflective attitude/shape configurations, the 90% and 95% quantiles should not differ too greatly from the median value.

However, for constellation satellites that glint more often or too brightly, or that more frequently employ brighter attitude/shape configurations, these quantiles will be expected to differ from the median value more significantly.

The solid red horizontal lines in Figure 1 show the maximum recommended brightness threshold magnitudes [2], calculated using eq. (1). Notably, for all three of the constellations studied here, most or all of the measured zenith magnitudes are brighter than this recommended threshold.

4.3.1 Starlink VisorSat Satellite Brightnesses

The median zenith range-normalized magnitude for the Starlink constellation estimated from the data plotted in Figure 1 is $M_z^{50} \approx 6.12$, which is 0.2 magnitudes fainter than the average value of 5.92 reported in an earlier study of MMT observations of VisorSat satellites [6], a relatively small difference compared to the overall level of variation for the combined data. The Starlink 90% quantile is $M_z^{90} \approx 4.92$, which is 1.2 magnitudes brighter than the median. This difference is due, in part, to the two or three brightest Starlink VisorSat light-curves plotted in Figure 1, which are each significantly brighter than M_z^{50} throughout their entire durations. No analysis has been performed in this study to understand the causes or nature of these occasional relatively bright light-curves. Figure 1 also indicates that 99.9% of the measured MMT zenith magnitudes for Starlink are brighter than the recommended maximum brightness threshold of $M_t = 7$. This brighter-than-recommended fraction at zenith is denoted as f_0 in this analysis.

4.3.2 OneWeb Satellite Brightnesses

The median for the OneWeb constellation estimated from the data in Figure 1 is $M_z^{50} \approx 7.67$, about 0.1 magnitude brighter than the average value of 7.58 reported in an earlier MMT study [5], again a relatively small difference compared to the overall level of variation. The OneWeb 90% quantile is $M_z^{90} \approx 6.80$, about 0.9 magnitudes brighter than the median. Notably, many of the individual light-curves for OneWeb satellites plotted in Figure 1 vary by 1.5 magnitudes or more during their duration. Figure 1 indicates that $f_0 = 65.7\%$ of the measured zenith magnitudes for OneWeb are brighter than the recommended threshold of $M_t = 7.85$.

4.3.3 Iridium 2nd Generation Satellite Brightnesses

The median for the Iridium 2nd Gen. constellation estimated from the data in Figure 1 is $M_z^{50} \approx 5.46$, and the 90% quantile is $M_z^{90} \approx 4.80$, about 0.7 magnitudes brighter. This makes individual Iridium satellites the brightest among the three studied constellations, as represented by the M_z^{50} and M_z^{90} metrics. Figure 1 also indicates that $f_0 = 100\%$ of the zenith magnitudes for this constellation are brighter than the recommended threshold of $M_t = 7.38$.

4.4 Representative Zenith Range-Normalized Magnitudes for Individual Constellation Satellites

For simplicity, this initial study employs a single zenith range-normalized magnitude, M_z^* , to characterize the brightness of a constellation's satellites. Specifically, this analysis chooses the measured 90% quantile for this characteristic magnitude, $M_z^* = M_z^{90}$, which serves as a reasonably conservative indicator of the potential contaminating effect that an individual constellation satellite might have on ground-based astronomical observations. For future analyses, other more or less conservative quantiles could be used as well (e.g., $M_z^* = M_z^{99}$ or $M_z^* = M_z^{70}$). The characteristic zenith magnitude can be expressed equivalently as a band-averaged flux, F_z^* , expressed in units of photons $\text{m}^{-2} \text{s}^{-1} \text{nm}^{-1}$. In the analysis to follow, fluxes from constellation satellites will be approximated using this conservative, statistically representative value, adjusted only to account for observer-to-satellite range variations.

5 FORMULATION OF CONSTELLATION METRICS

This study formulates expressions for a set of metrics that assess in different ways the potential risk of a constellation on visible and near-IR astronomy. These include the number of visible and illuminated satellites above ground-based observers, as well as the combined radiometric fluxes from those satellites. The methodology formulates statistically expected time-averaged estimates for these quantities, using two approaches. The first, more general approach considers a realistic, non-uniform distribution of constellation satellites. The second considers an idealized, uniform distribution, and allows the derivation of semi-analytical expressions that are relatively easy to calculate, but still provide reasonably accurate estimates for low-latitude observers.

5.1 Estimating the Number of Visible and Illuminated Satellites Above a Ground-based Observer

This section formulates expressions for the number of constellation satellites above a ground-based observer, restricted to regions of the sky within a specified angle of the zenith direction. The analysis uses $z = 60^\circ$ for this maximum zenith angle (which is equivalent to considering all observation elevation angles larger than 30°).

5.1.1 Line-of-Sight Integration through the Time-Averaged Spatial Density of Satellites

The statistically expected total number of satellites above a ground-based observer can be estimated by first integrating the time-averaged spatial density of the constellation along the line of sight (LOS) defined by zenith angle, θ , and azimuth angle, ϕ , and then integrating over solid angle, as follows

$$N_a = \int_0^z d\theta s_\theta \int_0^{2\pi} d\phi \int_{\rho_l}^{\rho_u} d\rho \rho^2 S(\mathbf{r}) \quad (3)$$

with ρ indicating the range from the observer along the LOS. (Note that this equation denotes the sine of the zenith angle as $s_\theta = \sin(\theta)$, a compact notation used for both sine and cosine functions used throughout this analysis.) The innermost integral represents integration along the LOS, with lower and upper range limits, ρ_l and ρ_u , which correspond to the bounds of the volume containing the constellation satellites, as described in more detail later. The two outer integrals in eq. (3) represent integration over solid angle. Taken together, the three integrals in eq. (3) also can be interpreted as integration over the volume of space above the observer occupied by the constellation satellites with zenith angles in the range $0 \leq \theta \leq z$. The integrand function, $S(\mathbf{r})$, represents the time-averaged spatial density of constellation satellites, also described in more detail later, and is expressed in eq. (3) as a function of the inertial position vector along the LOS, \mathbf{r} , as given by the following parametric equation

$$\mathbf{r} = \mathbf{r}(\rho, \phi, \theta) = \mathbf{r}_o + \rho \hat{\boldsymbol{\ell}}(\phi, \theta) \quad \text{with} \quad \hat{\boldsymbol{\ell}} = \hat{\boldsymbol{\ell}}(\phi, \theta) = \hat{\mathbf{n}}_o c_\phi s_\theta + \hat{\mathbf{e}}_o s_\phi s_\theta + \hat{\mathbf{r}}_o c_\theta \quad (4)$$

with \mathbf{r}_o indicating the position of the ground-based observer in the Earth-centered inertial (ECI) frame of reference, and $\hat{\boldsymbol{\ell}}$ the unit vector along the LOS, which is expressed using the observer's local horizon coordinate system north ($\hat{\mathbf{n}}_o$), east ($\hat{\mathbf{e}}_o$) and radial ($\hat{\mathbf{r}}_o$) unit vectors. (These latter three unit vectors can be constructed from \mathbf{r}_o , and because \mathbf{r}_o varies in time as the Earth rotates, these three ECI-frame vectors vary in time as well.)

The expected number of satellites above an observer that are also illuminated by the Sun can be expressed similarly

$$N_i = \int_0^z d\theta s_\theta \int_0^{2\pi} d\phi \int_{\rho_l}^{\rho_u} d\rho \rho^2 S(\mathbf{r}) I_s(\mathbf{r}, \mathbf{r}_s) \quad (5)$$

This integrand contains an extra factor, the binary function $I_s(\mathbf{r}, \mathbf{r}_s)$, which indicates the solar illumination status of a satellite at the position \mathbf{r} along the LOS, such that $I_s = 1$ when sunlit, and $I_s = 0$ otherwise. The function $I_s(\mathbf{r}, \mathbf{r}_s)$ can be evaluated analytically relatively easily by approximating the Earth as a sphere and the Sun as a point-source illuminator. Analytical evaluation is also possible but less straightforward for an oblate Earth (with polar radius ~22 km less than that of the equator), and for a solar disk of finite angular extent (which creates a penumbral shadow).

The number of all constellation satellites above an observer, N_a , is greater than or equal to the number of illuminated satellites, N_i . At sunset or sunrise, when the solar depression angle equals zero, all satellites above an observer are illuminated, so $N_a = N_i$. As discussed in more detail below, for low-altitude constellations, N_i tends to decrease quickly with increasing solar depression angle. For high-altitude constellations, however, N_i can remain almost as large as N_a well into astronomical night.

5.1.2 The Kessler Time-Averaged Spatial Density of Satellites

In 1981, Kessler [12] derived an expression for the time-averaged volumetric probability density function (PDF) of a single satellite orbiting an oblate central body

$$S_K(r, \beta) = \begin{cases} \left(2\pi r a [(r - q)(Q - r)(s_i^2 - s_\beta^2)]^{1/2} \right)^{-1} & \text{if } q \leq r \leq Q \text{ and } s_\beta^2 \leq s_i^2 \\ 0 & \text{otherwise} \end{cases} \quad (6)$$

which is written as a function of the inertial-frame radial distance, $r = |\mathbf{r}|$, and latitude, $\beta = \arcsin(\hat{\mathbf{z}} \cdot \mathbf{r} / r)$, but which also depends on the orbit's perigee distance $q = a(1 - e)$, and apogee distance $Q = a(1 + e)$, with a and e denoting the semi-major axis and eccentricity, respectively. The semi-major axis is $a = R_e + h$, with R_e equal to the equatorial radius of the Earth, and h the satellite's orbital altitude. Eq. (6) applies to prograde or retrograde orbits, with $i = \min(i_o, \pi - i_o)$ and i_o denoting the orbital inclination. The Kessler approximation idealizes the orbit as being perturbed only by Earth's J_2 gravitational term, and represents an average over time scales much longer than the J_2 -induced cyclical period of the right-ascension of the ascending node, Ω [12, 13]. Notably, even though the

function $S_K(r, \beta)$ diverges on the boundaries of the Kessler density volume, defined by $q \leq r \leq Q$ and $s_\beta^2 \leq s_i^2$, integrating the PDF over the entire volume yields a finite result of one (which can be done analytically).

The Kessler PDF can be used to estimate the statistically expected time-averaged spatial density of a constellation of satellites, idealized here all to have the same (a, e, i) orbital parameters

$$S(\mathbf{r}) = N_c S_K(r, \beta) \quad (7)$$

with N_c denoting the number of satellites in the constellation. Constellations distributed over a set of different orbital altitudes or inclinations can be modeled similarly using a weighted sum of Kessler functions. The integration limits for range, ρ_l and ρ_u , in eqs. (3) and (5) represent the intersections of the LOS with the two spheres that bound the Kessler volume. The lower limit is given by

$$\rho_l = \varrho(q, \theta, r_o) = b(q, \theta, r_o) - r_o c_\theta \quad \text{with} \quad b(q, \theta, r_o) = \sqrt{q^2 - (r_o s_\theta)^2} \quad (8)$$

and the upper limit is $\rho_u = \varrho(Q, \theta, r_o)$. The range function $\varrho(q, \theta, r_o)$ and associated function $b(q, \theta, r_o)$ will be used again later in the formulation.

Figure 2 plots N_a and N_i for the Starlink and OneWeb constellations, calculated by inserting the Kessler density of eq. (7) into eqs. (3) and (5), respectively, and numerically evaluating the resulting three-dimensional (3-D) integrals, assuming an oblate Earth figure and a point-source Sun. Specifically, the solid black lines show N_a calculated as a function of observer latitude for northern winter solstice observing conditions. The solid red lines show N_i calculated at the nearest time within ± 12 hours of solstice when the solar depression angle, α , is 24° . (Note that for latitudes less than about -40° , α remains below 24° for the entire 24-hour period bracketing N winter solstice.)

Figure 2 shows that both N_a and N_i calculated using the Kessler distribution vary significantly with observer latitude, reaching peak values near latitudes equal to the constellation's inclination. For the Starlink constellation, these peaks occur at latitudes of about $\pm 50^\circ$; for OneWeb the peaks occur over Earth's poles. (The curves for the Iridium constellation have similar shapes as those for OneWeb.) As can be seen in Figure 2, the peak values for N_a and N_i can exceed the corresponding low-latitude values by a significant factor (i.e., by about $\times 3$ for Starlink and $\times 7$ for OneWeb). Kessler-based estimates also vary somewhat from season to season.

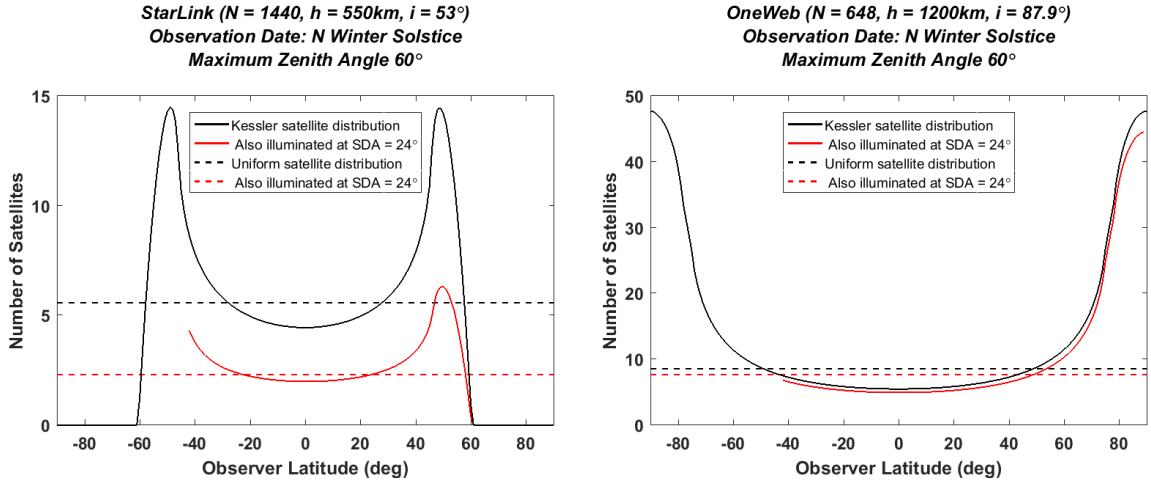


Figure 2. The number of visible and illuminated satellites as a function of observer latitude at northern winter solstice, within 60° of zenith, and for a solar depression angle of 24° , for the Starlink constellation (left) and OneWeb constellation (right).

5.1.3 The Uniform Thin Shell Approximation for the Spatial Density of Satellites

A simpler approximation for the spatial density assumes that the constellation satellites are distributed uniformly within a thin spherical shell over all latitudes, and results in a PDF of the form

$$S_U(r) \approx \begin{cases} V_U^{-1} & \text{if } q \leq r \leq Q \\ 0 & \text{otherwise} \end{cases} \quad \text{with} \quad V_U = \frac{4\pi}{3} (Q^3 - q^3) \approx 8\pi e a^3 \quad (9)$$

In this equation, V_U indicates the total volume of the spherical shell, which can be approximated as shown for $e \ll 1$. Using this PDF, the combined constellation's spatial density can be approximated as $S(\mathbf{r}) \approx N_c S_U(r)$, which allows considerable simplification of the expressions for both N_a and N_i . Specifically, approximating the Earth as a sphere and assuming $e \ll 1$, allows all three integrals in eq. (3) to be evaluated analytically, and results in a closed-form approximation for N_a which can be expressed in two equivalent ways

$$N_a \approx \frac{N_c}{2a} [a - R_e s_z^2 - c_z b(a, z, R_e)] = \frac{N_c}{2} \left[1 - \cos \left(z - \arcsin \left(\frac{R_e \sin(z)}{a} \right) \right) \right] \quad (10)$$

The first form, derived as part of this analysis, uses the function $b(a, z, R_e)$ defined in eq. (8). The second form was derived previously by Hainaut and Williams [1] using similar assumptions but a different methodology. (These two expressions can be shown to be equivalent by applying trigonometric identities.) The dashed black lines in Figure 2 show estimates calculated using this uniform thin shell approximation. Although this approach fails to reproduce the peaks at higher latitudes, for low latitudes it does approximately match the numerically integrated results plotted as the solid black curves. As previously noted [1], this approximation provides a reasonably conservative overestimate of N_a for most of the world's premier ground-based observatories, which are within $\sim 30^\circ$ of Earth's equator.

Additionally treating the Sun as a point-source allows the innermost two integrals in eq. (5) to be evaluated analytically (which can be done by using a reference frame that rotates the local horizon $\hat{\mathbf{n}}_o$ and $\hat{\mathbf{e}}_o$ axes, such that the rotated $\hat{\mathbf{n}}'_o$ axis aligns as much as possible with the observer-to-Sun vector). This yields the following uniform thin shell approximation for the number of illuminated satellites above an observer

$$N_i \approx \frac{N_c}{2\pi a} \int_0^z d\theta s_\theta \left\{ \frac{\phi_i(\theta, \alpha) [\varrho(a, \theta, R_e)]^2}{b(a, \theta, R_e)} \right\} \quad (11)$$

The function $\phi_i(\theta, \alpha)$ represents the half-width of the range of azimuth illuminated by sunlight, which is restricted to $0 \leq \phi_i \leq \pi$, and given by

$$\phi_i(\theta, \alpha) = \arccos(\gamma) \quad \text{with} \quad \gamma = \min(1, \max(-1, \gamma')) \quad \text{and} \quad \gamma' = \frac{s_\alpha(\rho c_\theta + R_e) - \sqrt{\rho(2c_\theta R_e + \rho)}}{\rho s_\theta c_\alpha} \quad (12)$$

In eq. (12), $\rho = \varrho(a, \theta, R_e)$ for brevity, and the solar depression angle is assumed to be in the range $0 \leq \alpha \leq \pi/2$. No convenient analytical solution for the integral in eq. (11) has been found, so it has been evaluated numerically in this analysis. (Note: in the limit $\alpha \rightarrow 0$, correctly calculated values for N_i should approach the values for N_a calculated from eq. (10). Also, care must be taken during the calculation in the limits $\alpha \rightarrow \pi/2$ or $\theta \rightarrow 0$, which results in $\gamma' \rightarrow \pm\infty$, but still should yield a definitive result for γ .) The dashed red lines in Figure 2 show estimates calculated using eq. (11), demonstrating again that, for low latitudes, the uniform thin shell approximation provides reasonably conservative overestimates of the more realistic Kessler-based results, plotted as the solid red curves.

5.2 The Time-Averaged Total Flux from Satellites Above a Ground-based Observer

The equations derived in the previous section provide estimates for the number of visible and illuminated constellation satellites above an observer, N_a and N_i , respectively. To incorporate the brightness of the constellation satellites, a similar approach can be used to estimate the total flux of photons from the constellation satellites above an observer within an angle z of the zenith direction. For visible and near-IR spectral bands dominated by reflected sunlight, this combined flux can be calculated by inserting another factor into the integrand of eq. (5) as follows

$$F_i = \int_0^z d\theta s_\theta \int_0^{2\pi} d\phi \int_{\rho_l}^{\rho_u} d\rho \rho^2 S(\mathbf{r}) I_s(\mathbf{r}, \mathbf{r}_s) F(\mathbf{r}, \mathbf{r}_s) \quad (13)$$

with $F(\mathbf{r}, \mathbf{r}_s)$ representing the flux reflected toward the ground-based observer by an individual satellite located at ECI position \mathbf{r} when illuminated by the Sun located at position \mathbf{r}_s . As discussed previously, $F(\mathbf{r}, \mathbf{r}_s)$ is also a complex function a great many other satellite-specific parameters [14]. This analysis approximates this function using the previously defined characteristic zenith range-normalized flux, F_z^* , but adjusted for observer-to-satellite range, so that $F(\mathbf{r}, \mathbf{r}_s) \approx F_z^*(h/\rho)^2$. Inserting this into eq. (13) yields

$$F_i \approx F_z^* h^2 \int_0^z d\theta s_\theta \int_0^{2\pi} d\phi \int_{\rho_l}^{\rho_u} d\rho S(\mathbf{r}) I_s(\mathbf{r}, \mathbf{r}_s) \quad (14)$$

For spectral bands that do not require solar illumination (e.g., thermal-IR), the analogous expression for F_a can be written by eliminating the factor $I_s(\mathbf{r}, \mathbf{r}_s)$ from the integrand in this equation. The total fluxes F_a and F_i also can be measured relative to F_z^* , as follows

$$F_a^{Rel} = F_a/F_z^* \quad \text{and} \quad F_i^{Rel} = F_i/F_z^* \quad (15)$$

These relative fluxes are dimensionless quantities, and can be thought of as the effective number of zenith-direction satellites that it would require to create the equivalent total flux from all of the constellation satellites distributed in the sky above an observer. The solid lines in Figure 3 plot F_a^{Rel} and F_i^{Rel} for the Starlink and OneWeb constellations, calculated using 3-D numerical integration over the Kessler-based density function.

Using the same uniform thin shell approximation approach described in the previous section, all three integrals for F_a can be evaluated analytically, yielding the following closed-form result

$$F_a^{Rel} \approx \frac{N_c h^2}{2aR_e} \left[\log_e \left(\frac{a+R_e}{R_e c_z + b(a, z, R_e)} \right) \right] \quad (16)$$

Similarly, the innermost two integrals for F_i can be evaluated analytically, yielding

$$F_i^{Rel} \approx \frac{N_c h^2}{2\pi a} \int_0^z d\theta s_\theta \left\{ \frac{\phi_i(\theta, \delta)}{b(a, \theta, R_e)} \right\} \quad (17)$$

which contains a 1-D integral evaluated numerically in this analysis. The dashed lines in Figure 3 plot F_a^{Rel} and F_i^{Rel} calculated using these two equations, demonstrating again that, for low latitude observers, the uniform thin shell approximation provides a reasonably conservative overestimate to the more accurate Kessler density results.

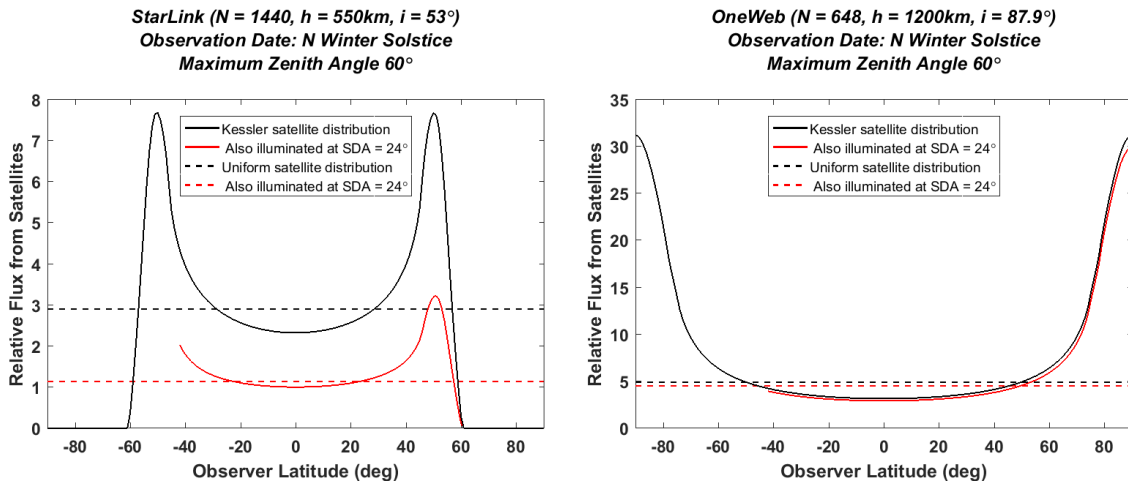


Figure 3. Relative flux as a function of observer latitude, from satellites within 60° of zenith, and for a solar depression angle of $\alpha = 24^\circ$ at N winter solstice, for the Starlink constellation (left) and OneWeb constellation (right).

5.3 Satellite Numbers and Fluxes as a Function of Constellation Altitude and Solar Depression Angle

Table 2 lists values for N_a , N_i , F_a^{Rel} , and F_i^{Rel} calculated as a function of constellation altitude and solar depression angle using the uniform thin shell approximation. Table 2 assumes a constellation population of $N_c = 1,000$ — meaning that the tabulated values also can be interpreted as per mil (‰) estimates (e.g., like a batting average in baseball). The color shading in Table 2 indicates the total number of illuminated satellites above a low-latitude observer within $z = 60^\circ$ of the zenith direction: green for $0 \leq N_i < 1$, yellow for $1 \leq N_i < 10$, and red for $N_i \geq 10$.

Table 2. Visible and illuminated satellites and total relative fluxes approximated for a constellation population of $N_c = 1,000$ and a maximum observation zenith angle of $z = 60^\circ$, tabulated as a function of constellation altitude (h) and solar depression angle (α).

h (km)	Twilight				Astronomical Night					
	Total Above Observer		Illuminated at $\alpha = 18^\circ$		Illuminated at $\alpha = 24^\circ$		Illuminated at $\alpha = 30^\circ$		Illuminated at $\alpha = 36^\circ$	
	N_a	F_a^{Rel}	N_i	F_i^{Rel}	N_i	F_i^{Rel}	N_i	F_i^{Rel}	N_i	F_i^{Rel}
250	0.96	0.47	0.13	0.04	0.00	0.00	0.00	0.00	0.00	0.00
300	1.34	0.67	0.52	0.24	0.00	0.00	0.00	0.00	0.00	0.00
350	1.77	0.89	1.02	0.53	0.00	0.00	0.00	0.00	0.00	0.00
400	2.24	1.14	1.58	0.85	0.14	0.05	0.00	0.00	0.00	0.00
450	2.74	1.41	2.19	1.19	0.52	0.21	0.00	0.00	0.00	0.00
500	3.29	1.70	2.84	1.53	1.03	0.46	0.00	0.00	0.00	0.00
550	3.87	2.02	3.51	1.89	1.60	0.79	0.00	0.00	0.00	0.00
600	4.47	2.36	4.20	2.26	2.24	1.18	0.26	0.09	0.00	0.00
650	5.10	2.72	4.91	2.65	2.92	1.59	0.67	0.26	0.00	0.00
700	5.76	3.09	5.63	3.05	3.63	2.03	1.18	0.50	0.00	0.00
750	6.44	3.48	6.36	3.46	4.37	2.48	1.75	0.80	0.00	0.00
800	7.13	3.89	7.10	3.88	5.14	2.94	2.38	1.16	0.15	0.05
900	8.58	4.74	8.58	4.74	6.73	3.90	3.77	2.00	0.94	0.38
1000	10.1	5.65	10.1	5.65	8.38	4.90	5.27	2.96	2.04	0.91
1100	11.6	6.61	11.6	6.61	10.1	5.93	6.85	3.98	3.32	1.63
1200	13.2	7.60	13.2	7.60	11.8	6.99	8.50	5.06	4.72	2.48
1300	14.8	8.63	14.8	8.63	13.5	8.08	10.2	6.17	6.22	3.44
1400	16.5	9.70	16.5	9.70	15.3	9.19	11.9	7.30	7.79	4.47
1500	18.1	10.8	18.1	10.8	17.1	10.3	13.7	8.46	9.41	5.57
1750	22.3	13.6	22.3	13.6	21.5	13.2	18.1	11.4	13.6	8.46
2000	26.5	16.5	26.5	16.5	25.9	16.3	22.5	14.5	17.9	11.5
2500	34.9	22.5	34.9	22.5	34.6	22.4	31.3	20.7	26.5	17.7
3000	42.9	28.6	42.9	28.6	42.8	28.6	39.7	26.9	34.9	23.9

Table 2 quantitatively demonstrates the key roles that the solar depression angle (α) and constellation altitude (h) have in the analysis. In fact, the interplay between these two variables shapes in an important way how much of an overall threat a constellation represents to ground-based astronomy [1-3]. This can be demonstrated by the following thought experiment: imagine the staff of a low-latitude observatory preparing for a night of observing of especially faint targets that are all within 60° of the zenith direction, using long-duration sensor exposures that could be irreversibly contaminated by too much flux reflected from an unanticipated intervening constellation satellite. In this scenario, the twilight period after sunset might be used for sensor setup and calibration. At the onset of astronomical night, when $\alpha = 18^\circ$, Table 2 indicates that 3.51% of the Starlink constellation's satellites ($h = 550$ km) would be expected to be sunlit within 60° of zenith. This fraction then decreases in time, to 1.60% for $\alpha = 24^\circ$, and to zero at $\alpha = 30^\circ$. At this point during astronomical night, observations could be conducted without any risk from the Starlink constellation. However, 13.2% of OneWeb constellation's satellites would be sunlit at the onset of astronomical night, decreasing only to 4.72% at $\alpha = 36^\circ$, and therefore represent a potential risk that persists much further into astronomical night. For higher altitudes constellations with $h \geq 1,500$ km the situation would be even worse: initially $\sim 20\%$ or more would be sunlit, and this fraction would remain comparably high well into, and possibly throughout, astronomical night. In this case, if the individual constellation satellites were too bright, the observatory staff would likely be compelled to use pre-tabulated constellation satellite ephemerides, if available, to schedule and/or interrupt the observations, in order to mitigate the risk of sensor exposure contamination [2].

The scenario described above indicates that the light pollution risk from higher altitude constellations is twofold: a larger fraction of the satellites are initially sunlit at the beginning of astronomical night, and a larger fraction remain sunlit into the night, thereby threatening the most valuable observation time available for many modes of ground-based astronomy. Even though the brightness of the individual high-altitude satellites might be lower due to their larger observer-to-satellite ranges, there is no way to eliminate this effect completely. For a constellation that simply must be deployed at such high altitudes, however, there are two ways of mitigating the effect: by decreasing the brightness of each satellite (through the use low-reflectance manufacturing designs or optimized on-orbit shape/attitude configurations), or by decreasing the total number of satellites in the constellation [2].

5.4 The Combined Constellation Magnitude: A Semi-Empirical Brightness Metric for Entire Constellations

The time-averaged total flux from illuminated satellites derived in the previous section is proportional to the individual satellite zenith flux as well as the constellation population, and can be expressed in the following form

$$F_i = F_z^* N_c G_i(\alpha, h, z) \quad \text{with} \quad G_i(\alpha, h, z) = F_i^{Rel} / N_c \approx \frac{h^2}{2\pi a} \int_0^z d\theta s_\theta \left\{ \frac{\phi_i(\theta, \alpha)}{b(a, \theta, R_e)} \right\} \quad (18)$$

with the function G_i representing the combined observational geometrical effects, which can be calculated using 1-D numerical integration when using the uniform thin shell density approximation, or 3-D numerical integration using the Kessler-based density approach. (Note, the columns labeled F_i^{Rel} in Table 2 also can be regarded as % measures of the function G_i estimated using the uniform thin shell approximation). Expressing the total flux in the form of a stellar magnitude yields

$$M_i = M_z^* - 2.5 \log_{10}[N_c] - 2.5 \log_{10}[G_i(\alpha, h, z)] \quad (19)$$

This “combined constellation magnitude” is the effective stellar magnitude of a single source that would produce a flux equal to F_i . As formulated here, this combined magnitude represents a reasonably conservative approximation of the flux of sunlight reflected towards a ground-based observer from all illuminated constellation satellites that are within an angle z of a ground-based observer’s zenith direction.

5.5 The Number of Satellites Brighter than the Recommended Limit: A Semi-Empirical Light Pollution Metric for Entire Constellations

Another metric that measures constellation light pollution is N_b , the statistically expected number of satellites above a ground-based observer that are also expected to be brighter than the recommended maximum brightness threshold. This metric can be formulated by inserting another binary factor into the integrand of eq. (5), which is equal to one if the satellite is predicted to be brighter than the threshold magnitude M_t , and zero otherwise. For the uniform thin shell approximation, this results in the following expression, which is also integrated numerically in this analysis

$$N_b \approx \frac{N_c}{2\pi a} \int_0^z d\theta s_\theta \left\{ \frac{\phi_i(\theta, \alpha) [\varrho(a, \theta, R_e)]^2}{b(a, \theta, R_e)} \right\} f(\theta) \quad (20)$$

with the function $f(\theta)$ indicating the fraction of constellation satellites observed at a zenith angle of θ that also have apparent magnitudes brighter than the recommended threshold. For $\theta = 0$, this equals the brighter-than-recommended fraction at zenith introduced in Section 4, i.e., $f_0 = f(0)$. Semi-empirical estimates for f_0 based on the MMT data are 99.9%, 65.7% and 100% for the Starlink, OneWeb and Iridium constellations, respectively. For $\theta > 0$, the brighter-than-recommended fraction $f(\theta)$ can be estimated by accounting for the expected change in apparent magnitude with the observer-to-satellite range, as follows

$$f(\theta) = \frac{1}{N_{obs}} \sum_{j=1}^{N_{obs}} U \left(M_t - M_{z,j} - 5 \log_{10} \left(\frac{\varrho(a, \theta, R_e)}{h} \right) \right) \quad \text{with} \quad U(x) = \begin{cases} 0 & x \leq 0 \\ 1 & x > 0 \end{cases} \quad (21)$$

with $M_{z,j}$ indicating the zenith magnitude derived from the j^{th} photometric observation, $j = 1 \dots N_{obs}$. At a zenith angle of $\theta = 60^\circ$, the MMT-based estimates for $f(\theta)$ are 26.9%, 9.6%, and 88.8%, for the Starlink, OneWeb and Iridium constellations, respectively, as calculated by applying eq. (21) to the data sets plotted in Figure 1.

5.6 Graphically Comparing Different Constellation Light Pollution Metrics

Figure 4 compares the M_i , N_i , and N_b metrics for the three studied constellations estimated using the uniform thin shell approximation and plotted as a function of solar depression angle (for $z = 60^\circ$). Notably, at the boundary between astronomical twilight and night, when $\alpha = 18^\circ$, the combined constellation magnitude, M_i , plotted on the left indicates that the Starlink constellation is collectively the brightest among the three. However, the middle panel indicates that the number of illuminated satellites above a low-latitude observer, N_i , is largest for OneWeb. The right panel shows yet a different pattern for that the number of brighter-than-recommended satellites, N_b . This comparison emphasizes that these three metrics provide different ways to measure constellation light pollution. Section 6 will present a constellation evaluation method based on the N_b metric, because it addresses the light pollution levels from satellites that exceed the currently recommended threshold brightness level.

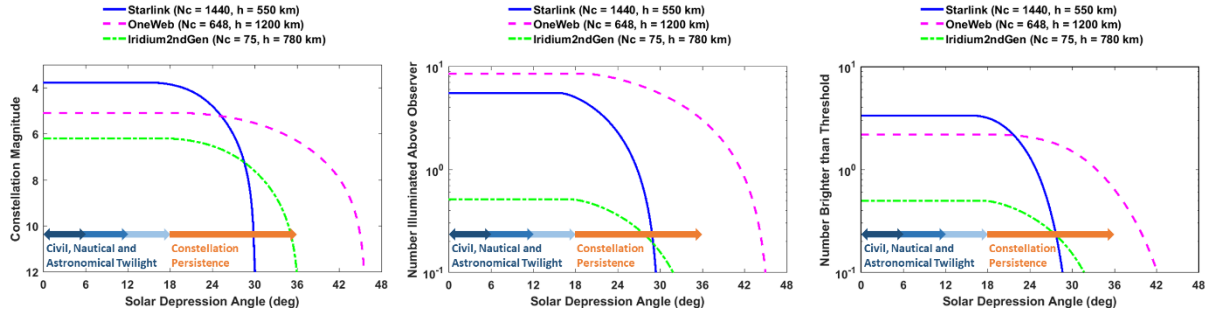


Figure 4. The combined constellation magnitude, M_i (left panel), the statistically expected number of sunlit satellites above an observer, N_i (middle), and the number of brighter-than-recommended satellites above an observer, N_b (right) for the three studied constellations. These metrics are each plotted as a function of the solar depression angle, α , and persist into astronomical night by varying amounts depending on the constellation’s altitude.

The curves in Figure 4 decrease as a function of solar depression angle, but at different rates. For instance, the left panel indicates that the Starlink constellation dims relatively quickly as α increases past 18° , and vanishes altogether at $\alpha \approx 30^\circ$. For $\alpha \geq 25^\circ$, the higher-altitude OneWeb constellation then becomes the brightest, as measured by the M_i metric, and remains so until $\alpha \approx 46^\circ$, after persisting further into astronomical night than the other two. When viewed in this graphical format, the curves can be considered to represent an extended “constellation persistence” period. Notably, all three metrics for the Starlink and Iridium constellations vanish at or before $\alpha \approx 36^\circ$, which might be considered a reasonable maximum limit for these kinds of light pollution indicators to persist at levels that could potentially affect ground-based astronomy — because this would limit the range for constellation persistence to $18^\circ \leq \alpha < 36^\circ$, which spans 18° just like the range spanned by natural twilight, and would leave periods of astronomical night with $\alpha \geq 36^\circ$ relatively unaffected by constellation light pollution.

5.7 The Probability of Contamination by Constellation Satellites During Astronomical Exposures

The same approach used to estimate the total flux from constellation satellites also can be used to estimate the probability that a particular astronomical target will be contaminated by sunlight reflected from one of the satellites as they drift across the sky above a ground-based observer. The formulation requires a multistep process, briefly described here. The first step is to insert another factor into the integrand of eq. (5), which represents the solid angle contaminated by a single constellation satellite during a time interval, T , the exposure duration for a ground-based sensor. This contaminated solid angle comprises two parts, $\Omega_T = \Omega_0 + T\dot{\Omega}$, with Ω_0 representing the solid angle contaminated by a constellation satellite during a very short duration exposure, and $\dot{\Omega}$ indicating the rate that additional solid angle is contaminated by the satellite as it drifts across the sky. After inserting Ω_T into the integrand of eq. (5), the resulting 3-D integral represents the total solid angle collectively contaminated by illuminated constellation satellites, Ω_i . This can then be divided by the total solid angle within the angle z of zenith to estimate the overall probability of contamination: $P_i = \Omega_i / [2\pi(1 - c_z)]$. For spectral bands not dominated by reflected sunlight, an analogous expression for P_a can be written that accounts for all constellation satellites above an observer, rather than just the illuminated ones. These two probabilities, P_a and P_i , can be calculated numerically using the Kessler-based density approach, and also simplified considerably using the uniform thin shell approximation, much as described in the previous sections for the four related quantities N_a , N_i , F_a , and F_i . A similar approach provides estimates for the probability of contamination exceeding a critical flux level, which would ruin an observation by overwhelming the signal from the desired astronomical target, or, alternatively, the

probability of sensor saturation. These probability of contamination indicators also can be plotted in the format shown in Figure 4, and represent yet another set of candidate metrics to evaluate constellation light pollution.

6 EVALUATING LIGHT POLLUTION RISKS FOR NEW OR PROPOSED CONSTELLATIONS

This section describes how plotting the metric N_b in the format used in Figure 4 provides a graphical means to evaluate the potential impact of new or proposed constellations, both in comparison to existing constellations, and in an absolute sense as well. Specifically, the process entails first predicting, $N_b(\alpha)$, the number of satellites expected to be brighter than the recommended threshold given in eq. (1) expressed as a function of solar depression angle, and then applying a two-part test to determine the associated potential effect on ground-based observations.

6.1 Comparing a New or Proposed Constellation to an Ensemble of Existing Constellations

The evaluation process can be demonstrated using a hypothetical scenario, by seeking an answer to the following query: If the three constellations listed in Table 1 and plotted in Figure 4 were the only ones that existed, would adding a specific new constellation significantly increase the risk to visible and near-IR ground-based astronomy conducted by low-latitude observers? Of course, any new set of satellites launched into orbit will have some effect, but this analysis uses the N_b metric (calculated with $z = 60^\circ$) to test for two specific types of light pollution impact, as evaluated by answering two more quantitatively addressable questions:

1. Would the new constellation have the largest N_b metric at any time during astronomical night?
2. Would the new constellation have a large N_b metric that persists too far into astronomical night?

The first question probes how the new constellation compares to others, in a relative sense. The second question addresses how the new constellation performs with respect to an absolute, predefined standard; specifically, it tests if the constellation is expected to produce more than a threshold number of brighter-than-recommended satellites beyond a maximum acceptable threshold solar depression angle. This study employs $N_t = 1$ for the threshold number of brighter-than-recommended satellites, and $\alpha_t = 36^\circ$ for the associated threshold solar depression angle, which could be considered a reasonable limit for the acceptable period for constellation light pollution to persist, as discussed previously. Using this α_t threshold, the second test only becomes a concern for proposed constellations with orbital altitudes above ~ 800 km; higher altitude constellations could still pass the test, but only by keeping the number or brightness of the satellites sufficiently low. (The α_t and N_t thresholds used in this study represent initial selections that seem to be both reasonable and conservative. Ideally, of course, such thresholds should be selected by consensus, through an effort that engages both the astronomical and constellation operator communities.)

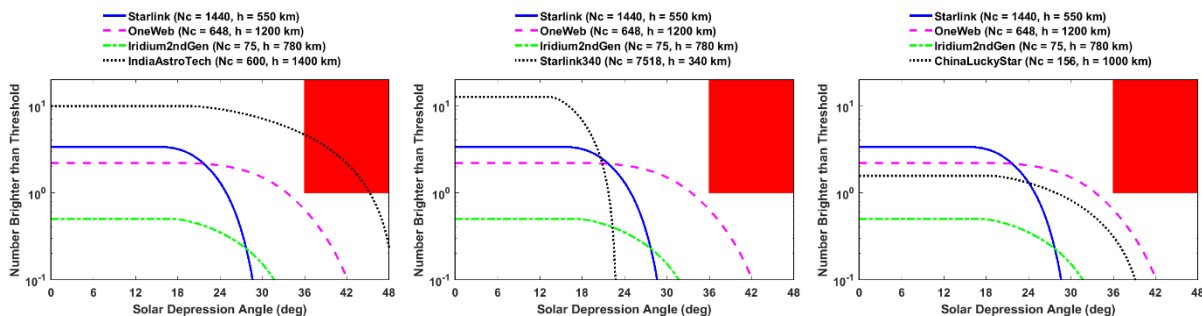


Figure 5. Number of satellites above a low-latitude observer exceeding the recommended brightness threshold for the three studied constellations, compared to those of three new constellations: the India AstroTech constellation (left), the Starlink 340 constellation (middle), and the China Lucky Star constellation (right).

Hainaut and Williams [1] analyze a large set of constellations, including the three studied here, plus several others that are mostly in the proposed or pre-launch phases of development (or are now obsolete). Figure 5 shows N_b metric comparisons for three of these other constellations. Each panel in Figure 5 shows the same three $N_b(\alpha)$ curves plotted in Figure 4, along with a new curve for one of the additional constellations. The region exceeding the thresholds $\alpha_t = 36^\circ$ and $N_t = 1$ is shaded in red in each panel. (Note: calculations for these hypothetical new constellations assume $f(\theta) = 1$ for simplicity, but $f(\theta)$ would have to be estimated more accurately for any actual light pollution evaluations for such proposed constellations.) The left panel shows the comparison for the idealized India AstroTech constellation, and an inspection of the N_b curve indicates that this new constellation would fail both light pollution impact tests: it fails the first because this constellation has a larger N_b metric than any of the pre-existing three; it fails the second because the N_b curve for this high-altitude constellation ($h = 1,400$ km) crosses the red shaded region. The middle panel in Figure 5 shows the comparison for the SpaceX Starlink-340 constellation,

which barely fails the first test, because it has a larger N_b than any of the pre-existing three for $18^\circ \leq \alpha \leq 21^\circ$, but passes the second because N_b vanishes at $\alpha \approx 23^\circ$ for this lower constellation ($h = 340$ km). The right panel in Figure 5 shows that the China Lucky Star constellation passes both tests.

The three comparison examples shown in Figure 5 demonstrate how this two-part testing method can be used to evaluate quantitatively the potential for a new constellation to become a significant source of light pollution for ground-based observers. For these hypothetical examples, only one of the three proposed new constellations would be found to be an acceptable light pollution risk: the China Lucky Star constellation (again, as evaluated on the basis of the N_b metric, and using the specific threshold values adopted here). The recommendation for the other two would be to change the constellation's population, altitude, and/or satellite design, in order to pass both parts of the test, and thereby mitigate the risk to ground-based visible and near-IR astronomy.

More or less conservative versions of this two-part test can be implemented by using different values for the α_t and N_t thresholds. Also, more sophisticated versions of the test can be implemented by using multiple criteria to define the conditions for high light pollution risk, resulting in a more complicated shape for the region shaded in red in each panel of Figure 5. For instance, a set of thresholds can be used to produce a sloped or saw-toothed shaped red region, which would provide a means of imposing light pollution limits that vary with solar depression angle.

6.2 Estimating Pre-Launch Brightnesses for Constellation Satellites

The two-part test described in the previous section relies on knowing or predicting the statistical distribution of constellation satellite brightnesses (such as the three distributions plotted in Figure 1). For the uniform thin shell approximation, the two-part test specifically requires estimates for the function $f(\theta)$, which statistically characterizes the fraction of constellation satellites with apparent magnitudes brighter than the recommended threshold when observed at a zenith angle of θ , as calculated using eq. (21). There are two primary ways that the required brightness distribution can be estimated before the launch of any satellites in a proposed constellation. The first is to build a software simulation model based on the constellation's actual satellite design that uses realistic and accurate bi-directional reflectance distribution functions for the surface materials, as recommended in previous constellation studies [2]. This model then could be used to simulate a statistically representative ensemble of ground-based light-curves, and estimate from those the associated $f(\theta)$ values, as described previously. A second method would be to use a set of currently orbiting satellites as analog objects, and adjust their observed brightness distributions to account for known differences between the analog and the constellation satellites.

As an example of the second method, consider the Starlink-340 constellation discussed by Hainaut and Williams [1] as a hypothetical example of a new constellation in the pre-launch phase of development. Assuming that this new Starlink constellation, with orbital altitude $h_{new} = 340$ km, deploys VisorSat design models and uses similar shape/attitude operational modes, then the new constellation's distribution of zenith fluxes and magnitudes could be estimated by scaling to correct for range-squared variations, as follows

$$F_{z,new} = F_z(h/h_{new})^2 \quad \text{and} \quad M_{z,new} = M_z - 5 \log_{10}(h/h_{new}) \quad (22)$$

with h , F_z and M_z representing values for current Starlink VisorSat satellites, used here as the analog objects. (In this case, this scaling adjustment would be applied to each of the black dots plotted in the left panel of Figure 1, in order to estimate the Starlink-340 constellation's brightness distribution.) If the new constellation's satellites were a different size, but otherwise similar in design to the analog satellites, then that effect could be approximately accounted for as well, e.g., by further scaling the observed fluxes by the ratio of the aspect-averaged projected reflective areas of the two satellite models. Additional adjustments could be used to account for other differences between the analog and pre-launch satellites. This approach could conceivably significantly alleviate the labor entailed in estimating pre-launch satellite brightness distributions, as long as an appropriate set of analog satellites could be identified, and corresponding ground-based photometric data were available.

Once the ground-based brightness distribution for a pre-launch constellation has been estimated using either of the methods outlined above, then eqs. (20) and (21) can be used to estimate the $N_b(\alpha)$ curve, which provides the means to perform the two-part test described in the previous section, in order to evaluate the new constellation's potential to affect ground-based astronomy too severely.

7 CONCLUSIONS AND FUTURE WORK

The various metrics formulated in this paper assess in different ways the potential impact of light pollution from satellite constellations on ground-based astronomy. These metrics include the time-averaged expected number of visible and illuminated satellites above a ground-based observer, N_a and N_i , the fluxes emitted by these satellites,

F_a and F_i , and a brief description of the associated probabilities of target contamination, P_a and P_i . The formulation also estimates N_b , the statistically expected number of constellation satellites above a ground-based observer that are also brighter than the currently recommended threshold for constellation satellites. These metrics are derived for realistic Kessler distributions of constellation satellites, as well as idealized uniform thin shell distributions. Analysis using the Kessler distribution indicates that these light pollution metrics for high-latitude ground-based observers can be significantly greater than those for low-latitude observers. The simpler uniform thin shell approximation provides reasonably conservative overestimates for low-latitude observers.

The statistically expected number of brighter-than-recommended constellation satellites above a ground-based observer, N_b , represents a single metric that simultaneously incorporates the effects of constellation population, altitude, brightness, and variability. For existing constellations, this metric is based on actual photometric brightness measurements. For proposed constellations, N_b could potentially be estimated using modeling and simulation in some cases, but in many others may require a semi-empirical approach that estimates pre-launch magnitudes by adjusting those observed for a set of currently orbiting analog satellites.

The two-part constellation evaluation test based on the N_b metric provides a quantitative method of comparing the potential impact that different constellations might have on ground-based visible and near-IR astronomical observations. Specifically, when plotted as function of solar depression angle, the $N_b(\alpha)$ curves can be analyzed graphically to evaluate a constellation's potential to affect ground-based observers, using a two-part test that incorporates both relative and absolute criteria. For the example evaluation criteria employed here, the second, absolute part of the test only becomes a concern for constellations with proposed altitudes above ~800 km; higher constellations can still pass the test, but only by keeping the number or brightness of the satellites sufficiently low.

In the future, other variants of this kind of light pollution evaluation method also could be investigated. This study focuses on using the number of brighter-than-recommended constellation satellites, N_b , as a metric to make the evaluation. However, other metrics could also be used to evaluate the potential impact of constellations in different ways — such as the probability of astronomical target contamination, for instance — which could be derived using the same methodology as presented here.

8 REFERENCES

- 1 Hainaut, O. P., and Williams, A. P., "Impact of Satellite Constellations on Astronomical Observations with ESO Telescopes in the Visible and Infrared Domain," *A&A*, v.636, p.A121, Apr 2020.
- 2 Walker, C., *et al.*, "Impact of Satellite Constellations on Optical Astronomy and Recommendations Toward Mitigations," *SatCon-1 Workshop Report*, NSF NOIRLab, Aug 2020.
- 3 Seitzer, P., "Large Constellations of LEO Satellites and Astronomy," The 2020 Technical AMOS Conference, Sep 2020.
- 4 Karpov, S., *et al.*, "Photometric Calibration of a Wide-Field Sky Survey Data from Mini-MegaTORTORA," *Astronomical Notes*, Special Issue: 15th INTEGRAL/BART Workshop, v.339, Jun 2018.
- 5 Malama, A., "The Brightness of OneWeb Satellites," *arXiv*, 2012.05100, Dec 2020.
- 6 Malama, A., "The Brightness of VisorSat-Design Starlink Satellites," *arXiv*, 2101.00375, Jan 2021.
- 7 Newman, L. K., "The NASA Robotic Conjunction Assessment Process: Overview and Operational Experiences," *Acta Astronautica*, Vol. 66, 2010, pp. 1253-1261.
- 8 National Aeronautics and Space Administration, "NASA Spacecraft Conjunction Assessment and Collision Avoidance Best Practices Handbook," NASA/SP-20205011318, Dec 2020.
- 9 Clark, S., "SpaceX launches more Starlink satellites, beta testing well underway," *SpaceFlight Now*, Sep 3, 2020 (retrieved from archive copy of the original web posting on Mar 1, 2021).
- 10 Graham, W., "Iridium Next-5 Satellites Ride to Orbit on SpaceX Falcon 9," NASA SpaceFlight.com, Mar 28, 2018 (retrieved from archive copy from the original web posting on Mar 1, 2021).
- 11 Cole, R. E., "A Sky Brightness Model for the Starlink "VisorSat" Spacecraft," *Research Notes of the AAS*, v.4, n10, p182, 2020.
- 12 Kessler, D. J., "Derivation of the Collision Probability between Orbiting Objects: The Lifetimes of Jupiter's Outer Moons," *Icarus*, v.48, p.39-48, 1981.
- 13 Vallado, D. A., *Fundamentals of Astrodynamics and Applications*, 2nd ed., Microcosm Press, El Segundo CA, 2001.
- 14 Hall, D., Calef, B., Knox, K., Bolden, M. and Kervin, P., "Separating Attitude and Shape Effects for Non-Resolvable Objects", *The 2007 AMOS Technical Conference Proceedings*, Kihei, HI, 2007.

Acknowledgements: The author would like to thank the CARA team for several helpful discussions.